Journal of Applied Polymer Science

Synthesis and characterization of PPY/K[Fe(CN)$_3$(OH)(en)] nanocomposite: Study of photocatalytic, sorption, electrical, and thermal properties

Syed Kazim Moosvi, Kowsar Majid, Tabassum Ara
Department of Chemistry, National Institute of Technology, Srinagar, Jammu and Kashmir 190 006, India
Correspondence to: K. Majid (E-mail: kowsarmajid@rediffmail.com)

ABSTRACT: This work involves the synthesis of nanocomposite of Polypyrrole (PPY) with photoadduct {K[Fe(CN)$_3$(OH)(en)]} via in-situ oxidative chemical polymerisation. Photoadduct is synthesized by irradiating equimolar mixture of potassium hexacyanoferrate (III) and ethylenediamine (en) and is then reduced to nanosize by high energy ball mill. Successful synthesis of nanophotoadduct is confirmed by elemental analyser, UV–Vis, and FTIR. The nanocomposite of PPY and photoadduct has been characterised by SEM, TEM, FTIR, XRD, TGA, UV–Vis spectroscopy, I–V characteristics, and dielectric analysis for structural, thermal, optical, electrical, and dielectric properties. The average particle size of nanophotoadduct and nanocomposite has been found to be 80 and 84 nm, respectively. The thermal stability of nanocomposite is enhanced. The nanocomposite shows high value of dielectric constant (5×10^3 at10^3 Hz) and ac conductivity (7.0×10^8 Sm^{-1} at 10^6 Hz) as compared with pure PPY. The high value of dielectric constant can make the material suited for energy storage applications. The nanocomposite shows higher photocatalytic activity as compared with pure PPY and a high value of distribution coefficient (K_d) has been obtained for Pb^{2+}, Zn^{2+}, and Cd^{2+} ions, hence, can act as an efficient material for removal of dyes and heavy metal ions in waste water. Thus, photoadduct of $K_3[Fe(CN)_6]$ and ethylenediamine(en), a new kind of filler, has succeeded in improving the properties of PPY with respect to thermal stability, high dielectric constant, high ac conductivity, efficient photocatalytic activity, and high K_d value for toxic metal ions. © 2016 Wiley Periodicals, Inc. J. Appl. Polym. Sci. **2016**, *133*, 43487.

KEYWORDS: composites; conducting polymers; thermal gravimetric analysis; irradiation

Received 3 November 2015; accepted 1 February 2016
DOI: 10.1002/app.43487

INTRODUCTION

Conducting polymers have become the subject of immense interest among material and academic researchers for the last few decades because of their interesting electronic, optical, and magnetic properties.[1] However, to tune the properties of these conducting polymers, composite science is essential. In this direction inorganic–organic composite materials have attracted intensive research, because of their potential to combine desirable properties of different constituent phases.[2] Organic part of composite imparts mechanical and chemical stability, whereas inorganic part of the composite supports the thermal stability, ion–exchange behavior, and electrical conductivity.[3] Ahead of this, nanomaterial synthesis and study, constitute an emerging subdiscipline in this conducting polymer area.[4] This class of new materials have numerous commercial and technological applications including analytical chemistry, drug delivery, bioencapsulation, optical, and electronic devices.[5] The creation of organic/inorganic nanocomposite with unique physical properties has attracted considerable interest due to their incredible properties, which arises from the synergism between the properties of their constituent phases.[6] Thus, conducting polymers have been explored in multidimensional ways and method.

Among these polymers, PPY is much studied polymer because of its unique properties, excellent environmental stability, ion exchange property, nontoxicity, low cost, and potential applications in electronic devices.[7–9] To amplify the applicability of PPY, various properties such as electrical, thermal, mechanical and electrochemical properties have been modified by incorporating nanostructured materials.[10] For example from literature survey, in PPY-NT/Ag nanoparticle nanocomposites, Ag nanoparticles have been found to enhance thermal stability, dielectric constant, and ac-conductivity of PPY.[11] PPY–Fe_2O_3 nanocomposite has been found to absorb microwave radiations.[12] The conductivity of PPY/Au nanocomposite has been found to be 12.6 S cm^{-1}.[13] PPY/Lanthanum strontium manganite oxide nanocomposite shows higher charge storage capacity than pure

PPY.[14] Incorporation of MWCNTs in the PPY matrix has been found to highly influence and enhance the electrical properties of the PPY matrix.[15] PPY/TiO_2 nanocomposite has been reported to show good photocatalytic activity for the degradation of methyl orange (MO) dye.[16] Therefore from literature it is obvious, that the properties of PPY can be tuned by the formation of nanocomposite with different fillers. The aim of this article is to synthesise a nanocomposite of polypyrrole (PPY) with nanophotoadduct of photoactive transition metal complex, namely, potassium hexacyanoferrate(III) and ethylenediamine ligand. Since photoadduct contains both organic and inorganic ligands, it can act as potent filler. Potassium hexacyanoferrate(III) has been chosen for its good photochemistry.[17–19] Ethylenediamine being a chelating ligand and good sigma donor can impart interesting properties in the photoadduct which in turn can retain in the nanocomposite. The material has been subjected to various characterization techniques. Thermal, electrical, dielectric, photocatalytic activity, and sorption study is reported in this article.

EXPERIMENTAL

Chemicals

Pyrrole was supplied by Himedia and was used after distillation. $K_3[Fe(CN)_6]$ and anhydrous ferric chloride was supplied by Fischer scientific. Ethylenediamine was supplied by Loba chemicals. All the reagents used were of analytical grade. All solutions were prepared in triply distilled water.

Physical Measurements

UV–Vis spectra were taken on double beam spectrophotometer (PG instruments T80). UV–Visible spectra of PPY and its nanocomposite were taken in DMSO solvent. FTIR spectra were recorded on Perkin Elmer RX – 1 FTIR spectrophotometer using KBr pellets. Irradiation was done with Osram UV photolamp. Surface morphology of the samples was taken on Hitachi FE - SEM Model S – 3600 N. X-ray diffraction was recorded on PW 3050 base diffractometer with Cu-Kα radiations ($\lambda = 1.54060$ Å). TEM was carried out with JEOL JEM-2100. For the sample preparation of TEM, a small amount of the powders was dispersed in few millimetres of ethanol through 30 min bath sonication. Thereafter, the dispersion was drop casted onto the copper grid. The samples were dried in a vacuum oven at ambient temperature for TEM characterizations.TGA/DTA of the samples was done using SDT Q 600 V 8.3 build 101 instrument in N_2 atmosphere at a heating rate of 10 °C min^{-1}. An aluminum pan was used as a reference. Dielectric study was carried out using Agilent 4285 A precision LCR meter in the range of 20 Hz–1 MHz. For this purpose the samples were compressed in the form of circular pellets by applying a pressure of 10 tons and coated with silver paste prior to electrical measurements. The thickness and diameter of the pellets were 2.35 and 10 mm, respectively. Photocatalytic study was carried out using Mercury-Xenon arc lamp and the experiments were carried out in dark.

Synthesis of Nanophotoadduct

To synthesise nanophotoadduct of $K_3[Fe(CN)_6]$, photolabilisation of ligands in $K_3[Fe(CN)_6]$ and their subsequent substitution with other ligands was carried out using Osram photo lamp. For this purpose an equimolar mixture of $K_3[Fe(CN)_6]$ and ethylenediamine was dissolved in water and irradiated for half an hour using Osram photolamp. The whole process was carried out in dark. Color of the mixture changed from yellow to greenish. The mixture was concentrated on water bath and cooled to room temperature. The product obtained was recrystallized for purification using water as solvent.Greenish colored crystals separated out which were subjected to various spectroscopic and surface characterizations. Obtained photoadduct was milled in high energy ball mill (PM 100) using 30 zirconium balls of 5 mm size for 16 hr at 450 rpm. The reduction of photoadduct to nanosize was confirmed from XRD and TEM.

Synthesise of PPY/Nanophotoadduct Composite

Nanocomposite of PPY with nanophotoadduct was synthesized by oxidative chemical polymerization using $FeCl_3$ as oxidant in nonaqueous medium. Solution of 0.055 mol $FeCl_3$ in 180 mL of chloroform was added to the stirring solution of 0.022 mol (in 70 mL chloroform) of distilled pyrrole monomer in a drop wise fashion. One gram of nanophotoadduct was then added to this mixture as filler for nanocomposite formation. The mixture was kept stirring for 24 h so as to disperse nanophotoadduct in the polymer solution. After 24 h of stirring black colored precipitate of nanocomposite was obtained after filtration which was then washed with methanol in order to remove remaining monomers and oxidants. The black powder was then dried in oven at 40–50 °C for 4 h.

Photocatalytic Activity

The photocatalytic efficiency of the PPY and nanocomposite of PPY with nanophotoadduct was studied for degradation of MO dye in presence of UV–Vis light using Mercury-Xenonarc lamp with the range of wavelength from 250 to 580 nm. The power of the lamp used was 470 watts. The distance between the lamp and the sample was about 12 cm. The intensity of the light near the solution surface was about 260 mW cm^{-2}. PPY (0.4 g) and nanocomposite was suspended into the 50 ppm aqueous solution of MO (200 mL). Before exposing the suspension to UV–Vis irradiation, they were stirred in dark for 40 min to attain adsorption–desorption equilibrium. Then, the suspension was irradiated under Mercury-Xenon arc lamp. At the given time intervals small aliquots from the suspension were taken out and separated by centrifugation. The absorbance of MO solution was then recorded at a wave length of 500 nm using double beam spectrophotometer (PG instruments T80).

Sorption Study

Various 100 mg portions of the exchanger in H^+ form were taken in Erlenmeyer flasks and 20 mL of different metal nitrate solutions in the required medium were added to each flask. After continuous shaking for 6 h, the flasks were kept for 24 h in a temperature–controlled incubator shaker at 25 °C to attain equilibrium. The amount of metal ions (Pb^{2+}, Zn^{2+}, and Cd^{2+}) in the solution before and after equilibrium, were determined by titrating against standard 0.001 *M* EDTA solution.

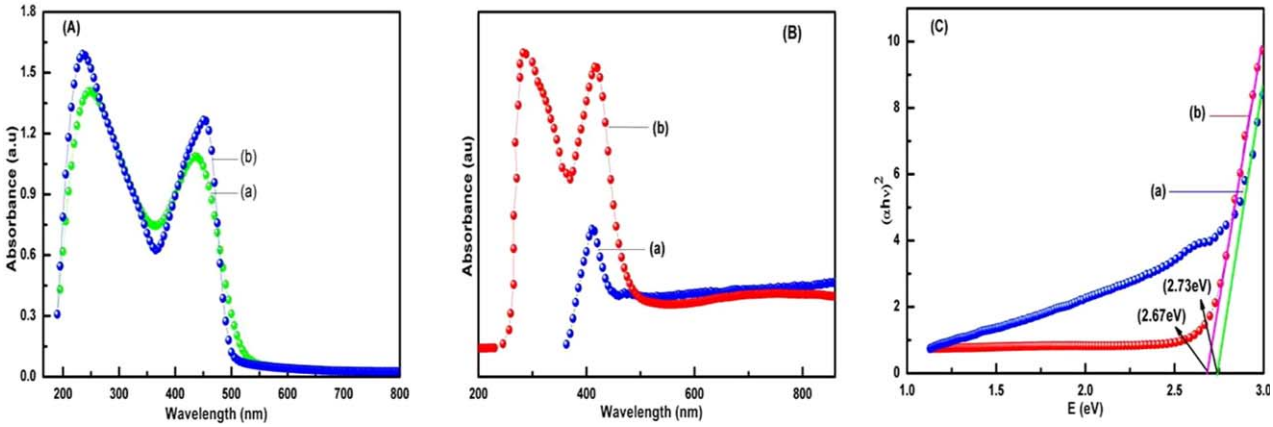

Figure 1. UV–Visible spectra of: (A) aqueous solution of $K_3[Fe(CN)_6]$ and ethylenediamine(en) (a) before irradiation and (b) after irradiation; (B) UV–Visible spectra of (a) PPY and (b) nanocomposite; (C) Tauc plot for determination of band gap (a) PPY (b) nanocomposite. [Color figure can be viewed in the online issue, which is available at wileyonlinelibrary.com.]

RESULTS AND DISCUSSION

Elemental Analysis

The complex formed between $K_3[Fe(CN)_6]$ and ethylenediamine(en) by photosubstitution process was analysed for C, H, and N and the empirical formula proposed for the complex was found to be $K[Fe(CN)_3(OH)(en)]$. The observed percentage of C, N, and H are 23.69, 26.74, and 3.45%, respectively, against the calculated percentages C = 24%, N =28%, and H = 3.6%.

UV–Visible Characterization

When aqueous $K_3[Fe(CN)_6]$ solution was irradiated with UV or visible light, Fe^{3+} and HCN was produced with increase in pH of solution. The pH of equimolar solution of $K_3[Fe(CN)_6]$and ethylenediamine was found to be 8.9 and 11.3 before and after irradiation, respectively. This increase in pH shows the successful photoaquation.[19] The irradiation results in the expulsion of cyanide ligands, which is replaced by aqua ligand as per the following reaction.[20,21]

$$[Fe(CN)_6]^{3-} \xrightarrow{hv} [Fe(CN)_5H_2O]^{3-} + HCN + OH^-$$

To confirm the expulsion of cyanide ligand from the $K_3[Fe(CN)_6]$ and its subsequent substitution by ethylenediamine, UV–Vis spectra was recorded before and after irradiation. As shown in Figure 1(A-a), the peaks observed before irradiation are at 245 and 435 nm, which are attributed to LMCT transitions.[18] These peaks show a shift after irradiation by appearing at 235 and 450 nm, respectively [Figure 1(A-b)].Thus a spectral change has occurred, which indicates ligand substitution.[19,22] Gloves, eye protection, and protective clothing should be worn during the synthesis of photoadduct.

UV–Visible Spectroscopy of PPY and Nanocomposite

Figure 1(B-a,b)] shows the UV–Vis spectra of PPY and its nanocomposite. The UV–Vis spectra of PPY shows a major absorption peak at 409 nm, which can be assigned to π-π^* inter band transitions.[23] This peak is red shifted to 420 nm in case of nanocomposite. This shift reflects the interaction between photoadduct and PPY chains in nanocomposite. Moreover, a shoulder at 288 nm and a hump called as broad free carrier band, from 600 to 850 nm is also observed. The peak at 288 nm is because of photoadduct since it shows its appearance in pure photoadduct at 235 nm. This shift reflects the interaction between photoadduct and PPY chains in nanocomposite. This is also supported by TEM micrographs. Since the material absorbs light in three major portions of electromagnetic spectrum, that is, ultraviolet, visible, and near IR regions, it can be efficiently used as a coating material on photoelectric material.

The energy band gap of polypyrole and its nanocomposite has been calculated with the help of absorption spectra using Tauc's relation.[24]

$$\alpha hv = A[hv - E_g]^n \quad (1)$$

where hv is energy of photon, h is planck's constant, α is absorption coefficient, E_g is optical energy gap, A is the constant, n is the index describing the electron transition process, which is related to density of states. It possesses discrete values, namely, 1/2, 3/2, 2, and 3 for direct allowed, direct forbidden, indirect allowed and indirect forbidden transitions.[25] From the plot of $(\alpha hv)^n$ versus hv a linear fit has been obtained for $n = 2$, thus indicating the transition to be indirect allowed in both PPY and nanocomposite. Optical band gap has been obtained by extrapolation of straight line to $(\alpha hv)^2 = 0$. Figure 1(C-a,b) shows the Tauc's plot of PPY and nanocomposite. Band gap for PPY and nanocomposite comes out to be 2.73 and 2.67 eV, respectively. This value of optical band gap shows the dielectric nature of material.

FTIR Characterization

FTIR spectra of $K_3[Fe(CN)_6]$, nanophotoadduct, PPY and nanocomposite are shown in Figure 2. FTIR of $K_3[Fe(CN)_6]$ exhibit peaks at (3464 and 1630 cm^{-1}), (2118, 2076, 2043) cm^{-1}, and 511 cm^{-1}, which are attributed to ν (OH) of lattice water (symmetric and antisymmetric), δ(H—O—H), ν(C≡N), and ν (Fe—CN) vibrational modes, respectively.[26] The FTIR bands observed for the photoadduct of $K_3[Fe(CN)_6]$ and ethylenediamine confirms the formation of photoadduct by showing characteristic peaks at (3582, 3430, and 3048), (2445, 2480, and 2508), 2041, 1619, 1517, (1387, 1320), 1256, 1158, 1106, 1063, 985, 822, 783, and 585 cm^{-1}, which are attributed to N—H

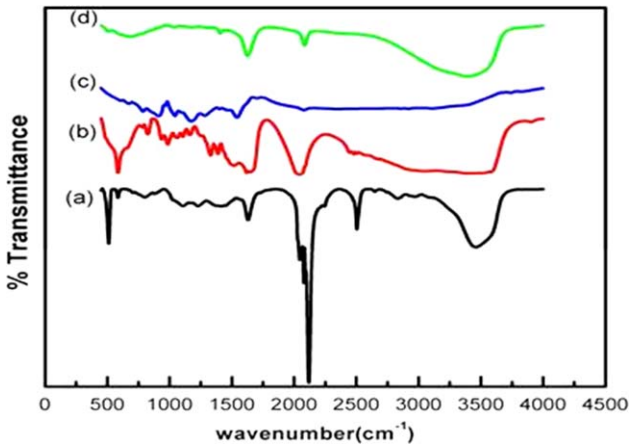

Figure 2. FTIR spectra of (a) $K_3[Fe(CN)_6]$, (b) nanophotoadduct, (c) PPY, and (d) nanocomposite. [Color figure can be viewed in the online issue, which is available at wileyonlinelibrary.com.]

stretching, C—H stretching, C≡N stretching, NH_2 bending, CH_2 bending, CH_2 wag, NH_2 wag, CH_2 twist, NH_2 wag, C—N stretching, NH_2 twist, C—C stretching, CH_2 rock, and Fe—CN stretching, respectively.[27] Moreover, the vibrational band due to N—H stretching vibration has become broad due to the presence of O—H vibrational band.

PPY exhibit characteristic peaks at 3391, 1536, 1444, 1297, 1041, 784, and 606 cm^{-1}, which are attributed to *v* (N—H), *v* (C—C), *v* (C=C), *v* (C—N), C—N in plane deformation mode, C—H and N—H in plane deformation vibration and C—H outer bending vibrations, respectively.[28] The insertion of photoadduct in the PPY matrix is evident by the appearance of a peak at 2083 cm^{-1}, which is due to *v* (C≡N). This peak appears at 2041 cm^{-1} in the nanophotoadduct with a strong intensity. This decrease in intensity and shifting of absorption peak by 40 cm^{-1} indicates the interactions of nanophotoadduct with PPY. Further the insertion of photoadduct in PPY is also evident by appearance of absorption peaks due to ethylenediamine with some shifts.

Thus from the discussion of FTIR of $K_3[Fe(CN)_6]$, nanophotoadduct, pure PPY and the nanocomposite of PPY with synthesized nanophotoadduct, the successful formation of photoadduct and its nanocomposite is evident.

XRD Characterization

XRD was recorded on PW 3050 base diffractometer with Cu Kα radiations (1.54060 Å). The XRD data has been analysed using powder X software. Figure 3(a–c) represent the XRD pattern of PPY, nanophotoadduct and nanocomposite. PPY shows a hump at $2\theta = 30°$; which shows amorphous nature.[29] XRD of nanophotoadduct shows sharp peaks, supporting crystalline structure. The XRD of nanocomposite shows the sharp peaks owing to the presence of nanophotoadduct in the polymer matrix. The presence of sharp intense peaks reflects more ordered arrangement in nanocomposite.[30] Moreover, a prominent peak at 2θ value of 30.7°, being a characteristic peak of photoadduct is observed in case of nanocomposite at 2θ value of 30° with a

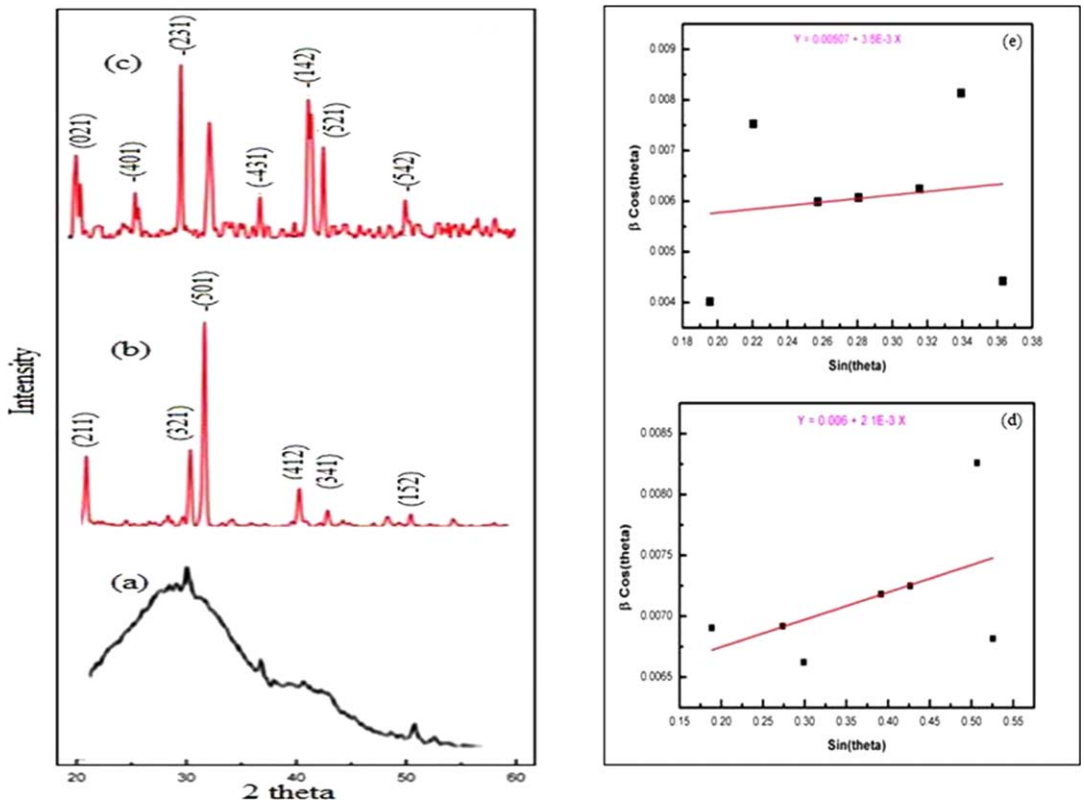

Figure 3. XRD of (a) PPY, (b) nanophotoadduct, (c) nanocomposite, and Williamson-Hall plot of (d) nanophotoadduct and (e) nanocomposite. [Color figure can be viewed in the online issue, which is available at wileyonlinelibrary.com.]

Table I. Parameters Evaluated from XRD of Nanophotoadduct of Potassium Hexacyanoferrate(III) and Ethylenediamine

h	*K*	*L*	Theta (obs)	*d* (exp)	*d* (cal)	Intensity
2	1	1	10.65421	4.16204	4.15915	58.8
3	2	1	15.38253	2.90181	2.90478	64.1
−5	0	1	16.03067	2.7874	2.78736	168.1
4	1	2	20.33726	2.21521	2.21497	32.0
3	4	1	21.63415	2.08830	2.08746	13.7
1	5	2	25.41409	1.79416	1.79438	10.8

slight shift due to interaction between PPY and photoadduct. Thus, on comparing PPY with nanocomposite, the appearance of distinct peaks shows the successful formation of an ordered nanocomposite.The lattice parameters have been calculated after refinement. The unit cell volume and R factor for nanophotoadduct comes out to be 1150.23972 and 0.00044, respectively, whereas for nanocomposite it is 1129.61263 and 0.00058, respectively. The value of calculated d spacing is in agreement with the experimental d spacing as shown in Tables I and II, respectively.

Moreover from the XRD of nanocomposite, it is clear that the photoadduct retains the monoclinic structure of potassium ferricyanide in the nanocomposite (JCPDS Number 83-2107), as the peaks observed for photoadduct appear in the XRD of nanocomposite, however, with some shifts.

Crystallite Size and Strain

The average crystallite size of nanophotoadduct and nanocomposite was calculated using Scherrer's formula.[31]

$$D = K\lambda/\beta\cos\theta \quad (2)$$

where D is crystallite size, K = shape factor (0.89), and λ = wavelength of Cu k_α radiation (1.54 A°). β is full width at half maximum and θ is the Bragg angle. From the calculations the average crystallite size of the nanophotoadduct and nanocomposite are found to be 20.398 and 24.833 nm, respectively. To find the relative contribution of particle size and lattice strain in the broadening of the XRD peaks, Williamson-Hall plot as shown in Figure 3(c,d) has been constructed. The Williamson-Hall equation is

$$\beta\cos\theta = k\lambda/D + 4\varepsilon\sin\theta. \quad (3)$$

where β is the full width at half maximum, k is Scherrer's constant; D is crystallite size, λ wavelength of X ray, ε lattice strain, and θ Bragg angle. β Cosθ is plotted against 4 Sinθ along Y and X axis, respectively, as shown in Figure 3(d,e) for nanophotoadduct and nanocomposite, respectively. Linear fit is applied to this plot, the crystallite size was estimated from the y- intercept $k\lambda/D$ and the strain (ε) was estimated from the slope of the fit. The scattering of points and hence poor fitting of the plots can be attributed to the anisotropy of the materials.[32] The size and microstrain obtained from W-H method are depicted in Table III. The size obtained using scherrer equation is less than that computed by Hall–Williamson method equation. This is attributed to the fact that the Scherrer equation does not take into consideration the effect of lattice strain and instrumental factors on peak broadening.[33] The crystallite size of nanocomposite obtained from both Scherrer equation and W-H plot method is more than the crystallite size of nanophotoadduct which can be due to agglomeration of nanocomposite particles. In addition, it can be due to the encapsulation of photoadduct by polymer matrix.

Surface Morphology

Surface morphology of PPY, nanophotoadduct, and nanocomposite is shown in Figure 4(a–c). SEM micrograph of PPY shows lumps with lot of grooves. This shows the amorphous nature of PPY. SEM micrograph of nanophotoadduct shows compact small pellet like structure. From the SEM micrograph of nanocomposite, the presence of nanophotoadduct is well evident, which supports successful synthesis of nanocomposite.

TEM images of PPY, nanophotoadduct and its nanocomposite are shown in Figure 5(a–c). PPY shows the presence of interconnected network like structure while nanophotoadduct shows agglomerated particles [Figure 5(a,b)].The TEM image of nanocomposite, however, shows the encapsulation of nanophotoadduct particles by PPY chains indicating the formation of

Table II. Parameters Evaluated from XRD Data of Nanocomposite of PPY with Nanophotoadduct of Potassium Hexacyanoferrate(III) and Ethylenediamine

H	*K*	*L*	Theta (exp)	*d* (exp)	*d* (cal)	Intensity
0	2	1	10.27584	4.31493	4.31661	162.7
−4	0	1	12.91221	3.44516	3.44644	84.3
−2	3	1	14.95150	2.98414	2.98324	328.2
−4	3	1	18.48408	2.42867	2.43071	82.7
−1	4	2	20.63823	2.18467	2.18603	265.6
5	2	1	21.31181	2.11872	2.11870	169.6
−5	4	2	24.96491	1.82455	1.82342	73.9

Table III. Lattice Parameters, Crystallite Size, Williamson – Hall, TEM Particle Size, and Microstrain of Nanophotoadduct and Nanocomposite

System	Crystal structure	Unit cell parameters	Cell volume	Crystallite size (nm)	Williamson Hall (nm)	TEM particle size (nm)	Strain × 10^{-4}
Nanophotoadduct	Monoclinic	$a = 13.96298$, $b = 10.36719$, $c = 8.30547$, $\alpha = \gamma = 89.8$, $\beta = 106.5$	1150.23	19.30	22.8	80	2.1
Nanocomposite	Monoclinic	$a = 13.91226$, $b = 10.30122$, $c = 8.26575$, $\alpha = \gamma = 89.9$, $\beta = 107.2$	1129.61	23.51	27	82	5.25

nanocomposite. Average particle sizes obtained from TEM image of nanophotoadduct and nanocomposite are found to be 80 and 82 nm, respectively. Moreover, the selected area electron diffraction (SAED) patterns of the nanophotoadduct and nanocomposite shows the presence of bright diffraction spots. The presence of bright spots in SAED pattern thus confirms the crystalline nature of photoadduct and nanocomposite.[34] Whereas SAED pattern of PPY depicts its amorphous nature, owing to the absence of bright spots. Presence of bright spots in SAED pattern of nanocomposite also supports the results obtained from XRD.

Thermal Analysis

Thermogram of nanophotoadduct and its nanocomposite are shown in Figure 6(a,b), respectively. Thermogram of PPY is showing 3% weight loss soon after the ambient temperature due to the removal of moisture. Then, the thermogram is stable up to 200°C, where from a steep decomposition takes place, which results in the weight loss of about 97% corresponding to the decomposition of whole PPY.[29] The decomposition stops at 580°C, where the residue left behind is zero. The thermogram of photoadduct is showing three transitions. The first transition starts from ambient temperature to 100 °C is due to the loss of water and two NH_2 moieties. The second transition that starts from 101 to 200°C with a mass loss of 21% corresponds to the removal of two cyanide moieties. The third transition starts from 600 to 900 °C is due to removal of hydroxide, two CH_2 moieties and one mole of KCN and rest is the residue left. The DTG curve reflects all the three transitions observed in thermogram. Furthermore, in all the transitions the observed weight loss is in accordance with the calculated weight loss. Figure 6(b) shows the thermogram of nanocomposite. Thermogram shows decomposition in three stages. The first stage of decomposition starts from ambient temperature to 100 °C, which may be attributed to the loss of absorbed water and unreacted monomer. The second stage starts from 100 to 200 °C, which is due to the loss of ligand moieties from the photoadduct. Then nanocomposite undergoes slow thermal degradation up to 550°C. The third stage of decomposition starts from 550 °C occurs steeply and is due to the degradation of polymer chain. On comparing the thermogram of PPY and its nanocomposite, it is clear that PPY undergoes complete decomposition at 580°C with 0% residual behind, while in case of nanocomposite, the weight loss at 580°C is 58% only. This indicates the enhanced thermal stability of nanocomposite in comparison to pure PPY. It is clear that induction of nanophotoadduct has increased the compact nature of the nanocomposite, due to which the degradation of PPY chain is supressed, thus leading to the increase in decomposition temperature.

Electrical Measurements

I–V characteristics of PPY and nanocomposite were recorded at room temperature as shown in Figure 7(a,b). The plots are found to be linear and hence show ohmic behavior. From the measured I–V characteristics of the sample the values of electrical conductivities have been found at room temperature. Following relation has been used for the determination of electrical conductivities.

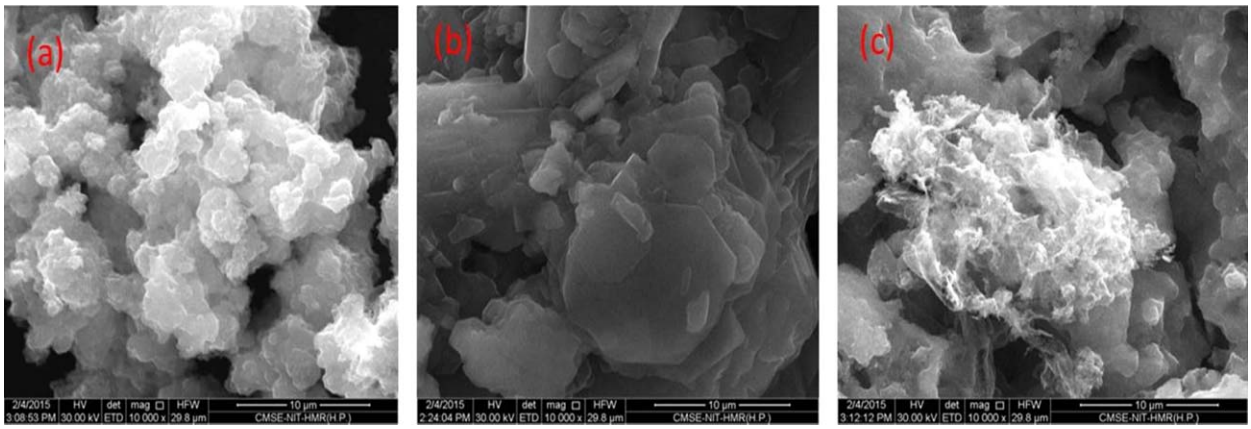

Figure 4. SEM micrographs of (a) PPY, (b) nanophotoadduct, and (c) nanocomposite. [Color figure can be viewed in the online issue, which is available at wileyonlinelibrary.com.]

$$\sigma=[(I\times L)/(V\times A)] \quad (4)$$

where I is the current, V the voltage, L the thickness, and A the cross-section area of sample.[35] The conductivity observed by four probe conductivity meter in case of PPY was found to be 5.38×10^{-7} S cm^{-1}, which has increased in case of nanocomposite to the level of 2.1×10^{-6} S cm^{-1}. This increase in conductivity can be attributed to the strong interfacial interactions between the PPy matrix and nanophotoadduct, as suggested by UV–Vis, FTIR, and XRD studies. These intermolecular interactions change the compact coil structure of PPY matrix to an

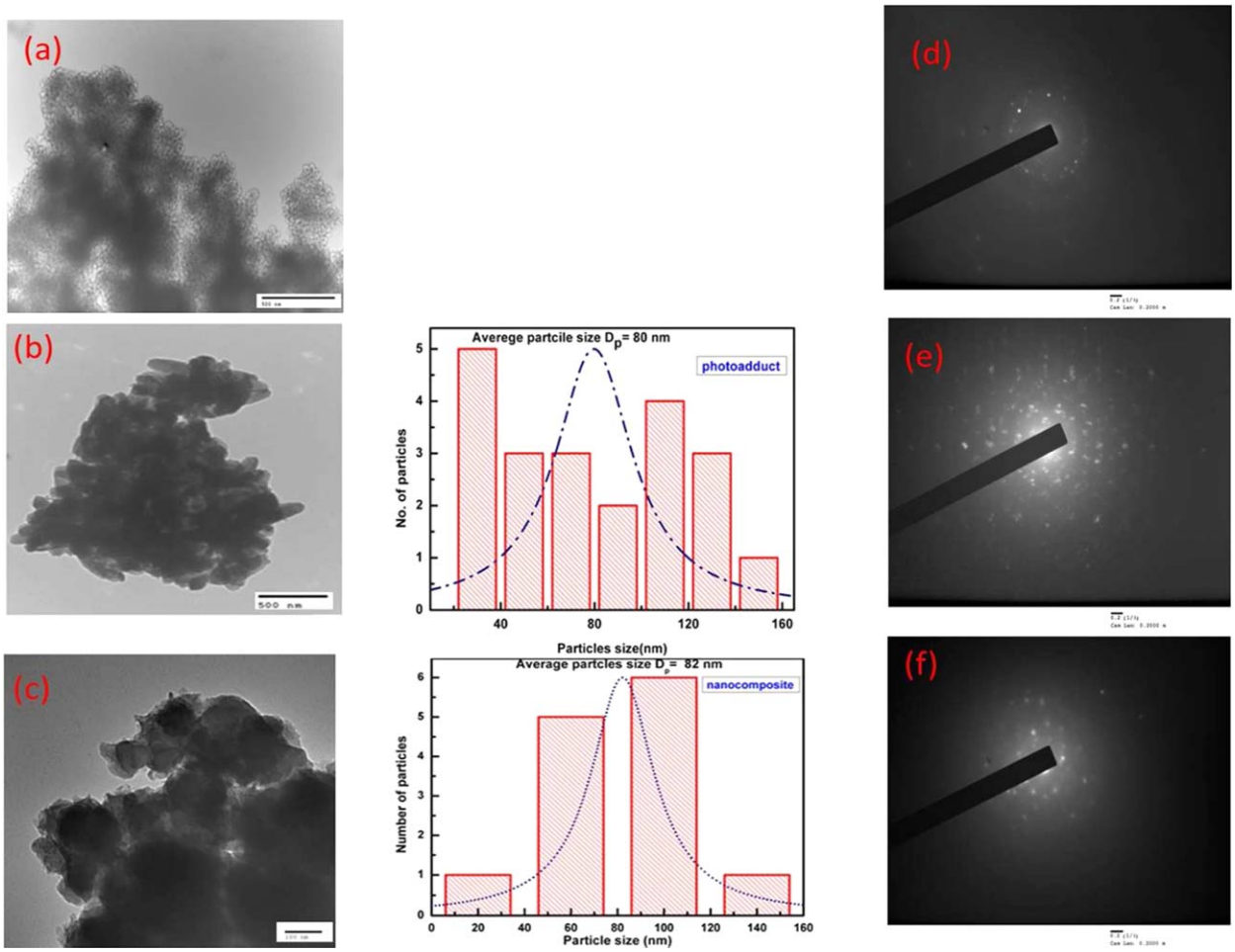

Figure 5. TEM micrographs of (a) nanophotoadduct, (b) PPY, (c) nanocomposite, and SAED of (d) PPY, (e) nanophotoadduct, and (f) nanocomposite. [Color figure can be viewed in the online issue, which is available at wileyonlinelibrary.com.]

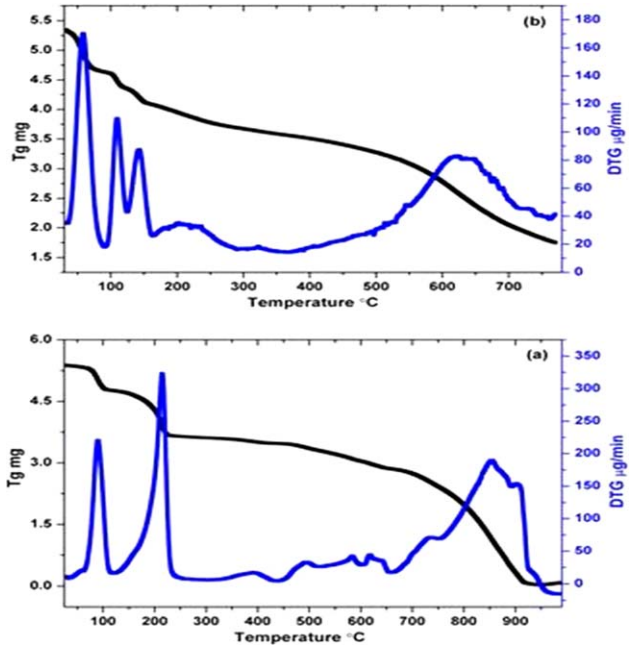

Figure 6. TGA/DTG of (a) nanophotoadduct and (b) nanocomposite. [Color figure can be viewed in the online issue, which is available at wileyonlinelibrary.com.]

expanded coil like structure. This uncoiling/stretching of polymer chain caused due to strong interfacial interactions between PPY matrix and nanophotoadduct tends to reduce π-conjugation defects in the polymer backbone and thus promotes linear conformation, which is necessary for crystallisation.[36] The degree of crystallinity of the polymer is thus increased, which ultimately leads to an enhancement in the conductivity of nanocomposite. One other reason for enhancement of conductivity could be the introduction of effective conductive paths to polymer matrix. The increase in crystallite size on formation of nanocomposite can be due to the encapsulation of nanophotoadduct by the polymer.

Dielectric Study

Dielectric response of synthesized nanocomposite of PPY has been carried out by Agilent 4285A precision LCR meter as a function of frequency of the applied ac field in the range of 20Hz-1MHz. Figure 8 shows variation of permittivity both ε′ (real part), ε″ (imaginary part), dielectric loss (tan δ), and ac conductivity (σ_{ac}) with the frequency of applied electric field. The parameters have been calculated by using following relations

$$\varepsilon' = C_p d/\varepsilon^\circ A \quad (5)$$

$$\varepsilon'' = \varepsilon' \tan\delta \quad (6)$$

$$\sigma_{ac} = 2\pi\nu\varepsilon'' \quad (7)$$

where C_p is the capacitance, d is the thickness of sample, ε° is the permittivity of the free space ($\varepsilon^\circ = 8.854 \times 10^{-12}\mathrm{Fm}^{-1}$), and A is the effective area.

Dielectric Constant

Figure 8(a,b) shows the variation of real and imaginary part of the dielectric constant of nanocomposite of PPY with nanophotoadduct. The nanocomposite shows the dielectric dispersion. The real part of dielectric constant decreases rapidly with increase in frequency in low frequency region while it shows almost frequency independent behavior at high frequency region. The imaginary permittivity as shown in Figure 8(b) also shows the similar behavior with the applied frequency. The dielectric constant of material depends on different types of polarization, namely, dipolar, electronic, atomic, and space charge polarization. A significant increase in the value of real and imaginary value of dielectric constant has been observed in nanophotoadduct doped PPY as compared to pure PPY.[37] This can be attributed to the orientation and interfacial polarisation due to the presence of K[Fe(CN)$_3$(OH)(en)] nanocrystals in the polymer matrix. The interfacial polarisation arises due to heterogeneous nature of nanocomposite, as the two phases of nanocomposite differ from each other in dielectric constant and conductivity.[38] Since the conductivity of the PPY matrix and filler is different, the mobility of charge carriers occurs more easily and randomly and these charge carriers get trapped at phase boundaries which lead to increase in dielectric constant (Maxwell Wagner interfacial model). These polarizations are operative at low frequencies. At low frequencies, the dipoles follow the field rapidly and therefore dipolar polarisations have maximum values and hence high value of dielectric constant (5×10^3 at10^3 Hz). The decrease in dielectric constant with increase

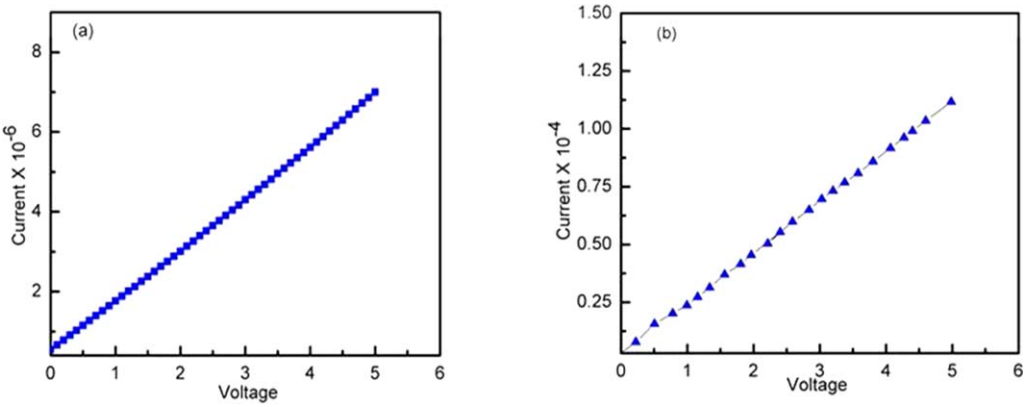

Figure 7. I–V characteristics of (a) PPY and (b) nanocomposite. [Color figure can be viewed in the online issue, which is available at wileyonlinelibrary.com.]

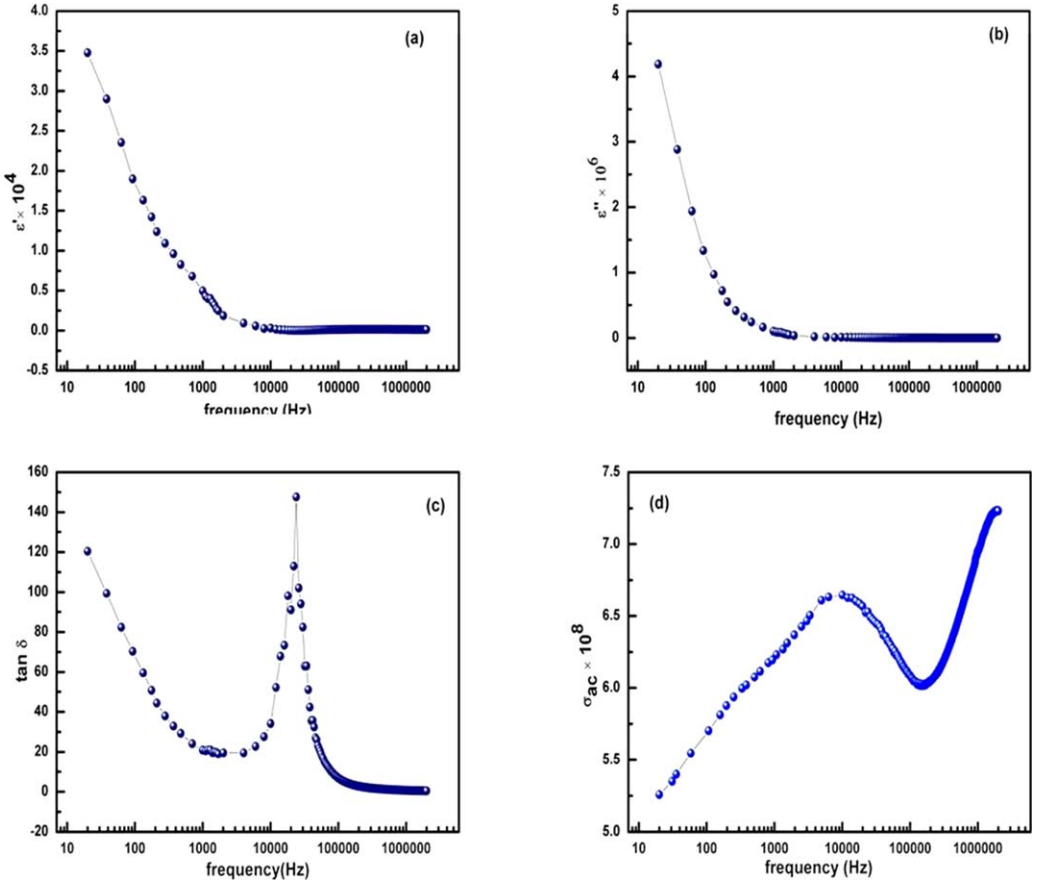

Figure 8. Variation of (a) real permittivity, (b) imaginary permittivity, (c) tangential loss, and (d) ac-conductivity with frequency. [Color figure can be viewed in the online issue, which is available at wileyonlinelibrary.com.]

in frequency is due to the decrease in orientation polarisation. The dipole orientation cannot keep up with the alternating field, the polarization direction is unable to remain aligned with the field and this polarization ceases to contribute to the polarization of the dielectric. The high value of dielectric constant obtained in the present material can be used to act as capacitor and hence in turn can be used for energy storage applications.

Dielectric Loss

Figure 8(c) shows the variation of dielectric loss with the applied field at room temperature. The dielectric loss is the dissipation of energy through the movement of charge carriers in an alternating electromagnetic field as polarization switches direction. Dielectric loss is especially high around the relaxation or resonance frequencies of the polarization mechanisms as the polarization lags behind the applied field. This causes an interaction between the field and the dielectric's polarization that result in heating. The tan δ in the nanocomposite has been found to decrease with increase in frequency. The frequency dependence of tan δ shows an anomalous behavior. A relaxation peak appears at higher frequency followed by subsequent decrease. This distribution of relaxation time is generally attributed to the difference in environments surrounding the different ions in the condensed material.[39] The condition for obtaining a maximum in the dielectric loss tangent of the material is given by the relation as shown below.

$$\omega\tau = 1 \tag{8}$$

where $\omega = 2\pi f$ and τ is relaxation time. Relaxation time is related to the jumping probability per unit time by the relation (9) and (10)

$$\tau = 1/2p \tag{9}$$

$$\text{or} f_{max}\ \pi p = 1 \tag{10}$$

Thus, from the above relation it is clear that the Debye relaxation process occurs when the jumping or hopping frequency of polarons and bipolarons approximately becomes equal to the applied field. At frequencies above 10^5 Hz the losses are found low, which identifies the possible application of this nanocomposite in high frequency device applications.

Ac Conductivity

Figure 8(d) shows the variation of ac conductivity (σ_{ac}) with the applied frequency at room temperature. The ac conductivity has been found to increase with increase in frequency. However, a peaking nature has been observed at around 10^4 Hz, this can be attributed to the presence of Debye relaxation peak as observed in dielectric loss [Figure 8(c)]. The total conductivity is the summation of band and hopping parts[40] as shown in relation:

$$\sigma_{total} = \sigma_0(T) + \sigma(\omega, T) \tag{11}$$

The first term is the Dc conductivity and the second term is the ac conductivity. The ac conductivity obeys the empirical relation.[11]

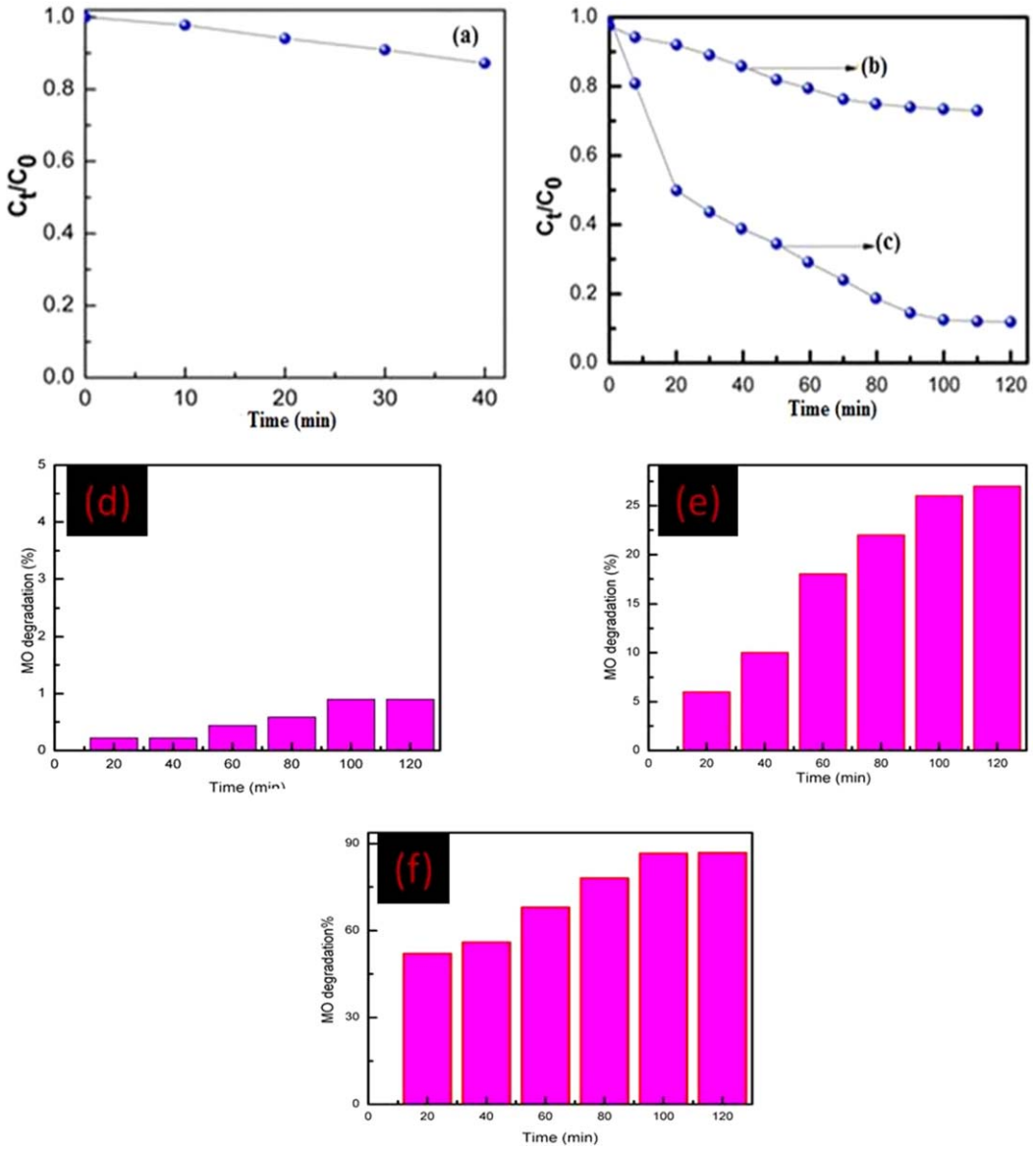

Figure 9. Plot of decrease in dye concentration C_t/C_0 with time in presence of (a) nanocomposite before irradiation. (b) In presence of PPY during irradiation. (c) In presence of nanocomposite during irradiation, Bar chart showing the % degradation of (d) MO as such (e) in presence of PPY and (f) in presence of nanocomposite, respectively. [Color figure can be viewed in the online issue, which is available at wileyonlinelibrary.com.]

$$\sigma_{ac}(w, T) = A(T)w^s \quad (12)$$

Where $A(T)$ is a constant generally, dependent on temperature and "s" is the frequency exponent and generally lies in the range $0 \leq s \leq 1$. The frequency exponent "s" has been obtained by plotting $\ln\sigma_{ac}$ versus lnw according to eq. (12). The value of "s" lies in the range of 0 and 1. When "s" = 0, the electrical conduction is frequency independent or DC conduction but for "s" ≤ 1 the conduction is frequency dependent or ac conduction. In our case, it is 0.1. The frequency dependence can be explained with the help of Maxwell Wagner heterogeneous model.[41] The increase in ac conductivity with applied frequency is because of the pumping force of the applied frequency which aids in transferring the charge carriers between the different localized sites as well as liberating the trapped charges from the different trapping centers.[39] Thus, we observe a gradual increase in conductivity with frequency.

The most important and interesting observation is that, the ac conductivity of samples is greater than pure PPY. Vishnuardhan *et al.* have reported that the ac - conductivity of pure PPY is 1.26×10^{-4} Sm^{-1} at 10^5 Hz[42] whereas for our sample it is 6.0×10^8 S cm^{-1} at the same frequency. Furthermore, the conductivity at 10^6 Hz is 7.0×10^8 Sm^{-1}, which indicates the formation of excess charge carriers (polarons and bipolaron) at higher frequencies. This increase in conductivity of nanocomposite as compared with PPY can be attributed to the improved microstructure on nanocomposite formation. The presence of nanophotoadduct in nanocomposite increases its orderness, which is confirmed from XRD and SEM. This orderness leads to an

improvement in the compactness and molecular orientations of composite material. The increase in the compactness of the material results in the improvement of the weak links between the grains. The coupling through the grain boundary become stronger and ultimately leads to an increase in macroscopic conductivity.

Photocatalytic Activity (Photodegradation of MO)

The % degradation of dye is calculated as

$$\%\text{Degradation} = \frac{c_o - c_t}{c_0} \times 100 \quad (13)$$

where C_0 is the initial concentration of dye before illumination and C_t after time t.[43]

During stirring of aqueous solution of MO dye and nanocomposite in dark for about 40 min, 5 mL aliquots of sample has been taken for analysis, which depicts slight decrease in absorption with time as shown in Figure 9(a). It may be due to the adsorption of MO dye on the surface of nanocomposite and hence depicts the development of adsorption–desorption equilibrium. The extent of degradation of MO dye in presence of PPY and nanocomposite was 27 and 86.8%, respectively, after 2 h. Anand *et al.* have reported 45% degradation of MO dye using Mn doped SnO_2 nanoparticles irradiated for the time period of 2 h.[44] This indicates that the synthesized nanocomposite can act as an efficient photocatalyst for degradation of MO dye. The enhancement in dye degradation by nanocomposite can be attributed to the synergistic interaction between PPY and nanophotoadduct, which improves the energy transfer. This leads to a higher concentration of electron/hole pair on the surface of a semiconductor and hence enhancing the photocatalytic activity.[43] The photocatalytic activity begins with the generation of electron/hole pair. When, a photocatalyst is illuminated by light with energy greater or equal to the band gap energy, the valence band electrons can be excited to the conduction band, leaving a hole in the valence band. Then these electrons and holes are transferred separately to the surface of the catalysts and react with the dye involved, leading to the formation of superoxide radical anions and hydroxyl radicals. These radicals are the reactive species in photocatalytic oxidation processes, which are recognized to be the most powerful oxidising species and hence attack organic material near the surface of the photocatalyst. A higher charge separation rate has been found beneficial to form these radicals, which favors the decoloration of MO.[44] The improved photocatalytic activity of nanophotoadduct doped PPY can be due to the introduction of the energy levels of nanophotoadduct in the conduction band of PPY. This can act as a mediator of interfacial charge transfer, thus leading to high separation rate of photoinduced charge carriers. Another possible reason for enhanced photocatalytic activity may be due to the large surface to volume ratio.

Several reports show that the rate of photodegradation of dyes fitted a pseudo first order kinetic model.[6]

$$\ln C_t - \ln C_0 = kt \quad (14)$$

$$\ln\left(\frac{C_t}{C_0}\right) = kt \quad (15)$$

where C_0 is the initial concentration and C_t is the concentration at any time (t), k is rate constant in min^{-1}. Figure 9(b,c) shows the plot of decrease in dye concentration (C_t/C_0) with time (min). The plot between C_t/C_0 and time (t) for PPY and nanocomposite suggests a pseudo first order reaction as shown in Figure 9(b,c). The value of k for nanocomposite is 6.8×10^{-3} and for PPY is 2.4×10^{-3}, which clearly indicates the enhanced photocatalytic activity of nanocomposite as compared with PPY.

Table IV. K_d Value of Nanocomposite of PPy with the Nanophotoadduct of $[K_3Fe(CN)_6]$ and Ethylenediamine

S. No.	Metal ion	K_d value (mL g^{-1})
1	Pb^{2+}	7200
2	Zn^{2+}	2700
3	Cd^{2+}	900

Distribution (Sorption) Studies

Distribution coefficient has been calculated by using the following relation:

$$K_d = \frac{I - F}{F} \times \frac{V(\text{mL})}{M(\text{g})} \quad (16)$$

where, K_d is the distribution coefficient (mL g^{-1}), I is the initial amount of metal ions in the solution phase, F is the amount of metal ions finally left in the solution after attainment of equilibrium, V is the volume of the solution, and M is the mass of ion exchanger (g).[45] Asif ali *et al.* has reported that the K_d value of PPY/Sn (IV) phosphate composite for Pb^{2+}, Zn^{2+}, and Cd^{2+} in DMW is 14, 10, and 1 (mL g^{-1}), respectively.[46] Similarly, K_d value of polyaniline/Sn(IV) phosphate composite for Cd^{2+} in DMW is 1169 mL g^{-1}.[47] Whereas, in this study, the K_d value of 7200, 2700, and 900 mL g^{-1} has been obtained for Pb^{2+}, Zn^{2+}, and Cd^{2+}, respectively, as shown in Table IV. Hence from the above study, it is clear that the synthesized nanocomposite can act as an efficient and potent adsorbent for Pb^{2+}, Zn^{2+}, and Cd^{2+} ions and thus can act as a promising material for waste water treatment.

CONCLUSIONS

A photochemical reaction between $K_3[Fe(CN)_6]$ and ethylenediamine was carried out to synthesize the photoadduct. The synthesized photoadduct was then subjected to ball milling for 16 h in planetary ball mill (PM = 100) using 30 zirconium balls of 5 mm size to reduce it to nanosize. This nanophotoadduct was then used in the synthesis of PPY nanocomposite via in-situ oxidative chemical polymerisation method. Nanodimensions of nanophotoadduct and nanocomposite was confirmed from XRD. Empirical formula of nanophotoadduct was found to be $K[Fe(CN)_3(OH)(en)]$ as confirmed by elemental analysis and TGA. Successful synthesis of nanophotoadduct and nanocomposite was proved by FTIR, SEM, and XRD analysis. Nanocomposite shows enhanced thermal stability and electrical conductivity as compared to pure PPY. The enhanced thermal stability allows the nanocomposite to be used in high temperature applications. Dielectric study shows that the dielectric constant and ac conductivity has increased by several orders of magnitude as compared to pure PPY. The large value of dielectric constant enables the material to be used for charge storage

purposes. The nanocomposite also exhibited good photocatalytic activity for MO dye and also shows excellent sorption efficiency for Pb^{2+}, Zn^{2+}, and Cd^{2+} ion in DMW, thus making it an excellent material for waste water treatment.

ACKNOWLEDGMENTS

The authors are thankful to Prof Rajat Gupta, Director NIT Srinagar, for help and support.

REFERENCES

1. Karim, M. R.; Yeum, J. H.; Lee, M. S.; Lim, K. T. *Mater. Chem. Phys.* **2008**, *112*, 779.
2. Kickelbick, G. *Prog. Polym. Sci.* **2003**, *28*, 83.
3. Mispa, K. J.; Subramaniam, P.; Murugesan, R. *J. Polym.* **2103**, *2013*, 1.
4. Ramanavicius, A.; Kausaitė, A.; Ramanaviciene, A. *Sens. Actuators B* **2005**, *111*, 532.
5. Li, Y.; Yu, Y.; Wu, L.; Zhi, J. *Appl. Surf. Sci.* **2013**, *273*, 135.
6. Kant, S.; Kalia, S.; Kumar, A. *J. Alloys Compd.* **2013**, *578*, 249.
7. Bouabdallah, A. B.; Djelali, N. E. *Rev. Roum. Chim.* **2014**, *59*, 627.
8. Madakbaş, S.; Çakmakc, E.; Kahraman, M. V.; Esmer, K. *Chem. Pap.* **2013**, *67*, 1048.
9. Su, N.; Li, H. B.; Yuan, S. J.; Yi, S. P.; Yin, E. Q. *Express Polym. Lett.* **2012**, *6*, 697.
10. Nandi, D.; Gupta, K.; Ghosh, A. K.; De, A.; Ray, N. R.; Ghosh, U. C. *Chem. Eng. J.* **2013**, *220*, 107.
11. Upadhyay, J.; Kumar, A. *Compos. Sci. Technol.* **2014**, *97*, 55.
12. Varshney, S.; Singh, K.; Ohlan, A.; Jain, V. K.; Dutta, V. P.; Dhawan, S. K. *J. Alloys Compd.* **2012**, *538*, 107.
13. Sun, L.; Shi, Y.; Li, B.; Chu, L.; He, Z.; Liu, J. *Colloids Surf. A* **2012**, *397*, 8.
14. Amarnath, C. A.; Ghamouss, F.; Schmaltz, B. *Synth. Met.* **2013**, *167*, 18.
15. Georgakilas, V.; Dallas, P.; Niarchos, D. *Synth. Met.* **2009**, *159*, 632.
16. Luo, Q.; Li, X.; Wang, D. *J. Mater. Sci.* **2011**, *46*, 1646.
17. Jordan, J.; Ewing, G. J. *Inorg. Chem.* **1962**, *1*, 587.
18. Alexander, J. J.; Gray, H. B. *J. Am. Chem. Soc.* **1968**, *90*, 4260.
19. Moggi, L.; Bolleta, V.; Balzani, F.; Scandola, J. *Inorg. Nucl. Chem.* **1966**, *28*, 2589.
20. Jimori, S. *Z. Anorg. Allgem. Chem.* **1927**, *167*, 145.
21. Lal, B. B.; Singhal, C. P. *Curr. Sci. India* **1944**, *13*, 78.
22. Van Grieken, R.; Aguado, J.; López-Munoz, M. J.; Marugán, J. *Appl. Catal. B* **2005**, *55*, 201.
23. Kepas, A.; Grzeszczuk, M.; Kvarnstrom, C.; Lindfors, T.; Ivaska, A. *Polish J. Chem.* **2007**, *81*, 2207.
24. Abdulla, H. S.; Abbo, A. I. *Int. J. Electrochem. Sci.* **2012**, *7*, 10666.
25. Mir, F. A.; Rehman, S.; Asokan, K.; Khan, S. H.; Bhat, G. M. *J. Mater. Sci. Mater. Electron* **2014**, *25*, 1258.
26. Nakagawa, I.; Shimanouchi, T. *Spectrochim. Acta* **1962**, *18*, 101.
27. Krishnan, K.; Plane, R. A. *Inorg. Chem.* **1966**, *5*, 852.
28. Najar, M. H.; Majid, K. *Synth. Met.* **2014**, *198*, 76.
29. Majid, K.; Tabassum, R.; Shah, A. F.; Ahmad, S.; Singla, M. L. *J. Mater. Sci. Mater. Electron* **2009**, *20*, 958.
30. Sangamesha, M. A.; Pushpalatha, K.; Shekar, G. L. *Indian J. Adv. Chem. Sci.* **2014**, 223. 227.
31. Jacob, R.; Nair, H. G.; Isac, J. *Int. Let. Chem. Phys. Astron.* **2015**, *41*, 100.
32. Kumari, S.; Singh, D. K.; Giri, P. K. *J. Nanosci. Nanotechnol.* **2009**, *9*, 5231.
33. Rehani, B. R.; Joshi, P. B.; Lad, K. N. *Indian J. Pure Appl. Phys.* **2006**, *44*, 157.
34. Deore, M. K.; Patil, N. U. *Int. J. Chem. Phys. Sci.* **2014**, *3*, 50.
35. Shaktawat, V.; Jain, N.; Saxena, R. J. *Optoelectron. Adv. Mater.* **2007**, *9*, 2130.
36. Pant, H. C.; Patra, M. K.; Negi, S. C. *Bull. Mater. Sci.* **2006**, *29*, 379.
37. Ozkazanc, E. *Synth. Met.* **2012**, *162*, 1016.
38. Tiwari, D. C.; Sen, V.; Sharma, R. *Indian J. Pure Appl. Phys.* **2012**, *50*, 49.
39. Dar, M. A.; Batoo, K. M.; Verma, V. *J. Alloys Compd.* **2010**, *493*, 553.
40. Dutta, P.; Biswas, S.; Ghosh, M. *Synth. Met.* **2001**, *122*, 455.
41. Irfan, M.; Shakoor, A.; Ali, B.; Elahi, A.; Tahra, Absar Ali, M. I. G. *Eur. Acad. Res.* **2014**, 2.
42. Vishnuvardhan, T. K.; Kulkarni, V. R.; Basavaraja, C. *Bull. Mater. Sci.* **2006**, *29*, 77.
43. Khan, J. A.; Qasim, M.; Singh, B. R. *Spectrochim. Acta Part A* **2013**, *109*, 313.
44. Anandan, K.; Rajendran, V. *Superlattices Microstruct.* **2015**, *85*, 185.
45. Rahman, N.; Haseen, U.; Rashid, M. Arab. J. Chem **2013**, http://dx.doi.org/10.1016/j.arabjc.2013.06.029. Accessed October 25, 2015.
46. Khan, A. A.; Khan, A.; Habiba, U. *J. Adv. Res.* **2011**, *2*, 341.
47. Khan, A. A. *Sens. Actuators B* **2006**, *120*, 10.